Semi-Annual Report Submitted to the
National Aeronautics and Space Administration

For July - December, 2001

Contract Number: NAS5-31370

Land Surface Temperature Measurements from EOS MODIS Data

MODIS Team Member
PRINCIPAL INVESTIGATOR

ZHENGMING WAN

P.I.'s Address:

Institute for Computational Earth System Science
University of California
Santa Barbara, CA 93106-3060

phone : (805) 893-4541
Fax no: (805) 893-2578
E-mail: wan@icess.ucsb.edu

Land Surface Temperature Measurements from EOS MODIS Data

Semi-Annual Report for July - December, 2001

Zhengming Wan

This report presents the status of Land-Surface Temperature (LST) standard products retrieved from Earth Observing System (EOS) Moderate Resolution Imaging Spectroradiometer (MODIS) data. Based on estimates of the channel-dependence error and noise equivalent temperature difference (NEDT) and the calibration accuracy of MODIS thermal infrared data, the impact of instrument performance on the accuracy of LST is discussed. A double-screen scheme based on the difference between the 5km LST retrieved by the day/night LST algorithm and the aggregated 1km LST retrived by the generalized split-window algorithm, and the difference between daytime and nighttime LSTs, is proposed to remove the LSTs contaminated with cloud effects. The accuracy of daily MODIS LST product at 1km resolution, which was produced by the generalized split-window algorithm, was validated in eleven clear-sky cases with in-situ measurement data collected in field campaigns in 2000 and 2001. The MODIS LST accuracy is better than 1K in the range from 263K to 300K over Lake Titicaca in Bolivia, Mono Lake, Bridgeport grassland, and a rice field in Chico, California, and Walker Lake, Nevada, in the atmospheric column water vapor range from 0.4 to 3.0cm. It is difficult to validate the daytime LST product over land sites rather than lakes with ground-based measurements alone because of the high spatial variations in the in-situ LST measurement data, which was verified by the daytime data of the MODIS Airborne Simulator (MAS) over a grassland in Bridgeport, California on 6 October 2000. In seven cases over a silt playa in Railroad Valley, Nevada, the 1km MODIS LSTs are a few Kelvin degrees lower than the in-situ measured LSTs because the surface emissivities inferred from land cover types in the split-window LST method are often overestimated in semi-arid and arid regions. After a correction with the difference between the 5km LST retrieved by the day/night LST method and the LST aggregated from 1km LSTs retrieved by the split-window method, the MODIS LSTs agree with in-situ measured LSTs within ±1K in the range from 263K to 322K for the seven cases in Railroad Valley and one case of snowcover in Bridgeport, California, leading a recommendation for use of the 5km LST product retrieved by the day/night LST method in bare and sparse vegetated areas.

Recent Papers

Z. Wan, Estimate of noise and systematic error in early thermal infrared data of the Moderate Resolution Imaging Spectroradiometer (MODIS), *Remote Sens. Environ.,* Vol. 80, pp. 47-54, 2002.

Z. Wan, Y. Zhang, Z.-L. Li, R. Wang, V.V. Salomonson, A. Yves, and R. Bosseno, Preliminary estimate of calibration of the Moderate Resolution Imaging Spectroradiometer (MODIS) thermal infrared data using Lake Titicaca, *Remote Sens. Environ.,* in press 2002.

X.-L. Ma, Z. Wan, C.C. Moeller, W.P. Menzel, and L.E. Gumley, Simultaneous retrieval of atmospheric profiles, land-surface temperature and emissivity from Moderate Resolution Imaging Spectroradiometer thermal infrared data: extension of a two-step physical algorithm, *Applied Optics,* in press 2002.

1. INTRODUCTION

Land-surface temperature (LST) is one of the key parameters in the physics of land-surface processes on regional and global scales, combining the results of all surface-atmosphere interactions and energy fluxes between the atmosphere and the ground (Mannstein, 1987; Sellers et al., 1988). One of the most important potential applications of the LST retrieved from satellite data is to validate and improve the global meteorological model prediction after appropriate aggregation and parameterization (Price, 1982; Diak and Whipple, 1993). Besides its necessity in the LST retrieval, the surface emissivity can be used to discriminate senescent vegetation (French et al., 2000a). The remotely sensed LST has been used in land cover and land-cover change analysis (Ehrlich and Lambin, 1996; Lambin and Ehrlich 1997) and in the production of the MODIS land cover product, in estimation and parameterization of surface fluxes (Brutsaert et al., 1993; French et al., 2000b), and in estimate the diurnal cycle (Jin and Dickinson, 1999). LST can be also used to monitor droughtness and estimate surface soil moisture (Feldhake et al., 1996; McVicar and Jupp, 1998), to evaluate water requirements of wheat (Jackson et al., 1977) and to determine frosts in orange groves (Caselles and Sobrino, 1989).

Remote sensing of sea surface temperature (SST) has been a primary function of satellite infrared radiometers since their inception. And starting from 1982, the SST derived from NOAA AVHRR (Advanced Very High Resolution Radiometer) data has been included in the high-resolution global SST climatology data set for global change studies (Brown et al., 1991; Smith and Reynolds, 1998). In comparison, there is no standard global LST data product derived from satellite remote sensing data even though the use of thermal-infrared (TIR) measurements for analysis of land biophysical conditions has been under investigation for more than three decades (Fuchs and Tanner, 1966) and the AVHRR data have been used to produce LST data in the development of LST algorithms for two decades. It is well known that simple extension of the SST methods to LST for AVHRR data would lead to unacceptable errors (Price, 1984; Becker, 1987) because of the difficulty in cloud detection with AVHRR data over land (especially for thin cirrus) and the intrinsic difficulties in the LST retrieval (Wan and Dozier, 1989).

The MODIS (Salomonson et al., 1989) onboard the first EOS platform (called Terra), which was successfully launched on 18 December 1999, provides a new opportunity for global studies of atmosphere, land, and ocean processes (King et al., 1992; Justice et al., 1998; Esaias et al., 1998), and for satellite measurements of global LST. The strengths of MODIS include its global coverage, high radiometric resolution and dynamic ranges suitable for atmosphere, land, or ocean studies, and accurate calibration in multiple TIR bands designed for retrievals of SST, LST and atmospheric properties. Specifically, band 26 will be used to detect cirrus clouds (Gao and Kaufman, 1995), band 21 for fire detection (Kaufman et al., 1998), all other TIR channels will be used to retrieve atmospheric temperature and water vapor profiles (Smith et al., 1985), and TIR bands 20, 22, 23, 29, 31-33 will correct for atmospheric effects and retrieve surface emissivity and temperature (Wan and Li, 1997). This report will present the heritage of LST

algorithms, the MODIS LST algorithms, a summary of performance of MODIS TIR bands and its impact on the accuracy of retrieved LST, a brief description of the MODIS LST products, and the LST validation results in the following sections.

2. HERITAGE FOR LST REMOTE SENSING

A variety of LST methods have been published in the open literature. Here we provide some examples rather than a complete review. LST can be retrieved from a single infrared channel through an accurate radiative transfer model if surface emissivity is known and temperature/water vapor profile is given by either satellite soundings or conventional radiosonde data (Price, 1983; Susskind et al., 1984; Chedin et al., 1985; Ottlé and Vidal-Madjar, 1992). Split-window LST methods require known surface emissivities to make corrections for the atmospheric and surface emissivity effects based on the differential atmospheric absorption in the 10-13μm split window without knowledge of the atmospheric temperature/water vapor profile although column water vapor is used in some split-window LST algorithms to improve the accuracy of LST retrieval (Price, 1984; Becker, 1987; Wan and Dozier, 1989; Becker and Li, 1990; Sobrino et al., 1991; Vital, 1991; Kerr et al., 1992; Ottle and Stoll, 1993; Prata, 1994; Wan and Dozier, 1996). Because the accuracy of LST retrieved by single channel methods and split-window methods depends on the accuracy of surface emissivity, these methods do not work well in semi-arid and arid regions, where surface emissivity may vary significantly with location and time.

Methods which extract relative emissivities from multispectral TIR data include reference channel method (Kahle et al., 1980), emissivity normalization method (Gillespie, 1985; Realmuto, 1990), TISI (temperature-independent spectral indices) method (Becker and Li, 1990), spectral ratio method (Watson, 1992), and alpha residuals method (Kealy and Gabell, 1990). Li et al. (1999) compares these methods with simulated TIMS (Thermal Infrared Multispectral Scanner) data, and shows that all these methods are sensitive to the uncertainties of atmosphere and an error of 20% in water vapor in mid-latitude summer atmosphere may lead to an error up to 0.03 in the relative emissivity in channel 1 of TIMS (at 8.379 μm), and the alpha method is even worse.

The TISI-based day/night method (Becker and Li, 1990) uses a pair of day/night co-registered AVHRR TIR data to estimate the bidirectional reflectance in channel 3, and then estimate emissivity in this channel based on the Lambertian assumption of surface reflectance (Becker and Li, 1990) or a priori knowledge of bidirectional reflectance distribution function (BRDF) (Li and Becker, 1993), emissivities in channels 4 and 5 with TISI, and finally estimate LST with the single channel method or the split-window method. If there are enough pairs of day/night co-registered AVHRR TIR data in a relative short period of time ranging from a few weeks to a few months depending on location and season in which surface BRDF does not change substantially and atmospheric temperature/water vapor profiles are available, directional emissivities at a series of view angles can be estimated using the integration of BRDF values in channel 3

estimated from AVHRR data (Nerry et al., 1998)

The temperature and emissivity separation algorithm for Advanced Spaceborne Thermal Emission and Reflection Radiometer (ASTER) (Gillespie et al., 1998) inherits features of the normalization method and spectral ratio method, and uses an empirical relationship of maximum-minimum emissivity difference (MMD) to refine estimates of surface emissivities and temperature.

In the above LST methods, only split-window methods do not require accurate atmospheric temperature/water vapor profile. Errors in emissivity and LST retrieved from all other methods depend on uncertainties in the input atmospheric profile. It is well known that there are large spatial and temporal variations in atmospheric water vapor. Padilla et al. (1993) made psychrometric measurements for study of atmospheric humidity behavior at two places in Mexico, one in the Chaoultepec Heights, in the western zone of Mexico City at 2300m above sea level, and another in Rancho Viejo, a mountainous wooded area at 2700m above sea level. The distance between these places is approximately 68km. They found that the mixing ratio mean values for clear-sky days in the 1989 rainy season vary 30% during 9:00-12:00 local time, and 40% in 12:00-15:00. Bruegge et al. (1992) reported that water vapor column abundances retrieved from the Airborne Visible Infrared Imaging Spectrometer (AVIRIS) data during the First ISLSCP Field Experiment (FIFE) over the Konza Prairie, Kansas, on 31 August 1990, indicated that the spatial variability over scales associated with surface topography and the underlying vegetation may be greater than 10%.

Because of the close coupling between land surface and atmosphere, small changes in surface emissivities cause measurable changes in infrared radiances so that uncertainties in surface emissivities may result in large errors in the atmospheric temperature/water vapor retrieval (Plokhenko and Menzel, 2000). Therefore, we have to consider the potentially large uncertainties in the atmospheric temperature/water vapor profiles retrieved from satellite TIR data when we use the atmospheric profiles in the estimates of land-surface emissivity and temperature, especially in areas where surface emissivities are in low values and highly variable.

3. MODIS LST ALGORITHMS

3.1 The Generalized Split-Window LST Algorithm

The LST of clear-sky pixels in MODIS scenes is retrieved with the split-window algorithm in a general form (Wan and Dozier, 1996)

$$T_s = C + (A_1 + A_2 \frac{1-\varepsilon}{\varepsilon} + A_3 \frac{\Delta\varepsilon}{\varepsilon^2}) \frac{T_{31} + T_{32}}{2} + (B_1 + B_2 \frac{1-\varepsilon}{\varepsilon} + B_3 \frac{\Delta\varepsilon}{\varepsilon^2}) \frac{T_{31} - T_{32}}{2} \quad , \qquad (1)$$

where $\varepsilon = 0.5(\varepsilon_{31} + \varepsilon_{32})$, and $\Delta\varepsilon = \varepsilon_{31} - \varepsilon_{32}$ are the mean and the difference of surface emissivities in

MODIS bands 31 and 32. T_{31} and T_{32} are brightness temperatures in these two split-window bands. The coefficients C, A_i and B_i, $i = 1, 2, 3$ are given by interpolation on a set of multi-dimensional look-up tables (LUT). The LUTs were obtained by linear regression of the MODIS simulation data from radiative transfer calculations over wide ranges of surface and atmospheric conditions. Improvements for the generalized split-window LST algorithm incorporated in the establishment of the LUTs include: 1) view-angle dependence, 2) column water vapor dependence, and 3) dependence on the atmospheric lower boundary temperature. The view-angle dependence is kept in one dimension of LUTs for a set of viewing angles covering the whole MODIS swath so that LST can be retrieved at higher accuracies for pixels at both small and large viewing zenith angles, and at best accuracies for pixels at nadir and small view angles. The column water vapor dependence is kept in another dimension of LUTs for a set of overlapping intervals of column water vapor so that the information of water vapor provided in the MODIS atmospheric product is used as the most likely range of the water vapor rather than its exact value because the uncertainties in the atmospheric water vapor may be large. Similarly, the information of the atmospheric lower boundary temperature (T_{air}) provided in the MODIS atmospheric product is also used to improve the LST retrieval accuracy. The LST accuracy can be improved further by iterations with the information of difference between surface temperature T_s and T_{air}.

The band emissivities, also called classification-based emissivities (Snyder et al., 1998), are estimated from land cover types in each MODIS pixel through TIR BRDF and emissivity modeling (Snyder and Wan, 1998). A simple linear correction is made to the band emissivities to account for the viewing angle effect in the emissivities when the viewing angle is larger than 45 degrees for some land cover types. In the at-launch MODIS LST processing, the University of Maryland IGBP-type land-cover based on AVHRR data (Townshend et al., 1994) is used to provide global land cover information at 1km grids. Since June 2001, the MODIS land-cover product (Muchoney et al., 1999) is used in the MODIS LST processing. Note that errors and uncertainties in the classification-based emissivities may be large in semi-arid and arid regions because of the large temporal and spatial variations in surface emissivities and lack of knowledge on the emissivity variation with viewing angle.

3.2 The MODIS Day/Night LST Algorithm

A physics-based day/night algorithm (Wan and Li, 1997) was developed to retrieve surface spectral emissivity and temperature at 5km resolution from a pair of daytime and nighttime MODIS data in seven TIR bands, i.e., bands 20, 22, 23, 29, and 31-33. The inputs to this algorithm includes the MODIS calibrated radiance product (MOD021KM), geolocation product (MOD03), atmospheric temperature and water vapor profile product (MOD07), and cloudmask product (MOD35). To our knowledge, this day/night algorithm is the first operational LST algorithm capable of adjusting the uncertainties in atmospheric temperature and water vapor profiles for a better retrieval of the surface emissivity and temperature without a complicated complete retrieval of surface variables and atmospheric profiles

simultaneously (Ma et al., 2000; Ma et al., 2002). Because we use a pair of daytime and nighttime MODIS data in seven bands, we have 14 observations. In the day/night algorithm, there may be maximum of 14 unknown variables. The minimal set of the surface variables includes 7 band emissivities, and daytime and nighttime surface temperatures. There are only five unknowns left for atmospheric variables. Because of the close coupling between land surface and atmosphere, uncertainties in surface emissivities may result in large errors in the atmospheric temperature/water vapor retrieval (Plokhenko and Menzel, 2000). These errors could exist in the shape of the retrieved temperature/humidity profile, and in the values of atmospheric temperature at the surface level (T_a) and column water vapor (cwv). Atmospheric radiative transfer simulations show that the MODIS radiances in the above seven TIR bands are relatively less sensitive to changes in the shapes of temperature and water vapor profiles. Therefore, we set four atmospheric variables (T_a and cwv, for daytime and nighttime, respectively). Then there is only one unknown left for the anisotropic factor of the solar beam BRDF at the surface. This anisotropic factor is defined by the ratio of the surface-reflected solar beam at the view direction of the MODIS sensor to the radiance that would have resulted if the surface reflected isotropically (such a surface is called Lambertian surface),

$$\alpha = \frac{\pi f_r(\mu; \mu_0, \phi_0)}{r} \quad , \tag{2}$$

where r is reflectance of the assumed Lambertian surface. Bidirectional reflectance measurements of sands and soils (Snyder et al., 1997b) show that although there are quite strong spectral variations in surface reflectance for most terrestrial materials in the 3.5-4.2μm wavelength range, their BRDF anisotropic factor in this wavelength range has very small variations on the order of 2%. Therefore, we can use a single anisotropic factor for bands 20, 22, and 23. Besides we assume: 1) The surface emissivity changes with vegetation coverage and surface moisture content. However, it does not significantly change in several days unless rain and/or snow occurs during the short period of time - particularly for bare soils in arid and semi-arid environments, for which the surface of the ground is normally dry (Kerr et al., 1992). 2) Atmospheric radiative transfer simulations show that in clear-sky conditions the surface-reflected diffuse solar irradiance term is much smaller than the surface-reflected solar beam term in the thermal infrared range, and the surface-reflected atmospheric downward thermal irradiance term is smaller than surface thermal emission. So the Lambertian approximation of the surface reflection does not introduce significant error in the 3-14 μm thermal infrared region. Then we can link hemispherical directional reflectance $r(\theta)$ to directional emissivity $\varepsilon(\theta)$ by $r(\theta) = 1 - \varepsilon(\theta)$ according to Kirchhoff's law. Based on the above assumptions, the radiance measured in MODIS band j can be expressed as

$$L(j) = t_1(j)\,\varepsilon(j)\,\mathrm{B}_j(T_s) + L_a(j) + L_s(j) + \frac{1-\varepsilon(j)}{\pi}\left[t_2(j)\,\alpha\,\mu_0\,E_0(j) + t_3(j)\,E_d(j) + t_4(j)\,E_t(j)\right], \tag{3}$$

where all terms are band-averaged, $\varepsilon(j)$ is the surface emissivity, $\mathrm{B}_j(T_s)$ is the radiance emitted by a

blackbody at surface temperature T_s, $L_a(j)$ is the thermal path radiance, $L_s(j)$ is the path radiance resulting from scattering of solar radiation, and $E_0(j)$ is the spectral solar irradiance incident on the top of the atmosphere (normal to the beam). $E_d(j)$ and $E_t(j)$ are the band-averaged solar diffuse irradiance and atmospheric downward thermal irradiance at the surface, and $t_i(j)$, $i = 1, \ldots, 4$ are the band effective transmission functions weighted by the band response function, the corresponding radiance, and irradiance terms. Note that we have neglected the in-band spectral variation of the surface emissivity in reducing a general integral equation into eq. (3), and have omitted symbols of view angle and solar angle for most terms in the above equation. On the right-hand side of this equation, $\varepsilon(j)$, α, and $B_j(T_s)$ depend on surface properties and conditions. All other terms depend on atmospheric water vapor and temperature profiles, solar angle and viewing angle. These terms can be given by numerical simulations of atmospheric radiative transfer. The set of 14 nonlinear equations in the day/night algorithm is solved with the least-squares fit method (Wan and Li, 1997).

Considering the angular variation in surface emissivity, we separate the whole range of MODIS viewing zenith angle into sub-ranges, and use one emissivity in each of the sub-ranges. In the day/night LST processing, we select a pair of clear-sky daytime and night MODIS observations at view angles in a same sub-range whenever it is possible. If there is no such pair of day/night observations available in a reasonable short period of time but there is a pair of day/night observations in different sub-ranges of view angle, we use this less favorable pair for surface emissivity and temperature retrieval and set a lower quality for the retrieved results. Sometimes we have to make a tradeoff between a favorable period of time and a favorable pair of view angles for temporal variations versus angular variations in surface emissivities. If the time difference between daytime and nighttime observations is too long, the chance for a large change in surface emissivity will be high. In the new product generation executive (PGE) code (version 3), the whole range of MODIS viewing zenith angle is separated into four sub-ranges (0° - 40°, 40° - 52°, 52° - 60°, 60° - 65°, respectively), instead of two sub-ranges in the earlier versions.

4. PERFORMANCE OF MODIS TIR BANDS

The specification and estimated performance of the TIR bands in the MODIS Proto-Flight Model (PFM) flown on Terra are shown in Table I. The channel-dependent noise and systematic error in MODIS TIR channel data were evaluated with early MODIS data over lake and ocean sites in clear-sky days acquired with the A-side of scan mirror and electronics before the end of October 2000 (Wan, 2002). In 14 cases of sub-area sites with a size of 10 lines by 16 pixels each line, where the brightness temperature in band 31 changes within ± 0.1K, average and standard deviation values of brightness temperatures in ten channels (consisting a ten-element linear detector array) of 16 MODIS TIR bands show the channel-dependent noise and systematic errors. It is found that the ninth channel in bands 21 and 24, and the fourth channel in band 22 are too noisy to use, and that the specification of noise equivalent temperature difference (NEDT) is reached in all other channels of the 16 MODIS TIR bands. There are significant channel-dependent

systematic errors in 1-3 channels in bands 22, 23, 25, 27-30. After a simple correction of the channel-dependent systematic errors with the statistics in the above 14 cases, the quality of the MODIS TIR data is significantly improved in bands 22-25, and 27-30, and the NEDT specification is reached or nearly reached in all bands as shown in column 5 of Table I.

The absolute radiometric accuracy of MODIS TIR channel data was evaluated with in-situ data collected in a vicarious calibration field campaign conducted in Lake Titicaca, Bolivia, during May 26 and June 17, 2000 (Wan et al., 2002). The comparison between MODIS TIR data produced by the new Level-1B code (version 2.5.4) and the band radiances calculated with atmospheric radiative transfer code MODTRAN4.0 (Berk et al., 1999) based on lake surface temperatures measured by five IR radiometers deployed in the high-elevation Lake Titicaca, and the atmospheric temperature and water vapor profiles measured by radiosondes launched on the lake-shore on 13 and 15 June 2000, calm clear-sky days, shows good agreements in bands 29, 31 and 32 (within an accuracy of 0.5%) in daytime overpass cases. Sensitivity analysis indicates that the changes on the measured atmospheric temperature and water vapor profiles result in negligible or small effects on the calculated radiances in bands 20-23, 29, and 31-32. Therefore, comparisons for these bands were made for cases when lake surface temperature measurements were available but no radiosonde data were available, and in sub-areas of 10 by 16 pixels where there was no in-situ measurement but MODIS brightness temperatures in band 31 vary within ±0.15K by using the validated band 31 to determine lake surface temperatures. These comparisons show that the specified absolute radiometric accuracy of 1% is reached or nearly reached in MODIS bands 21, 29 and 31-33, and that there is a calibration bias of 2-3% in bands 20, 22, and 23. The error analysis also shows that the radiosondes cannot provide accurate atmospheric temperature and water vapor profiles to estimate the calibration accuracies in the atmospheric sounding bands at the specified 1% level and that the calibration accuracy in the ozone band (band 30) cannot be estimated without in situ measurements of ozone. Column 6 in Table I shows the estimated values of calibration bias, which are averaged from sub-areas with viewing zenith angles smaller than 50 ° in June 13 and 15.

The MODIS sensor was reconfigured on 31 October and 1 November 2000 to the B-side Science Mode from the A-side Science Mode (see Terra PFM Instrument Status and Terra MODIS History on webpage http://mcstweb.gsfc.nasa.gov/Home.html). By transiting to latest focal plane bias voltage in the B-side configuration, the three originally noisy detector elements returned to normal performance. The MODIS instrument experienced a Power Supply 2 shutdown anomaly and did not take science data during the time period of June 15 to July 2, 2001. The MODIS instrument was reconfigured to the A-side Science Mode with the same focal plane bias voltage used in the B-side mode on 3 July 2001. The MODIS data in this configuration are referred as new A-side data. To evaluate the calibration accuracy of the new A-side data, we conducted a field campaign in Walker Lake, Nevada in mid October 2001. The size of Walker Lake is approximately 20km long in the S-N direction and 7km wide in the E-W direction. The lake surface elevation is 1196m above sea level. On 18 October 2001, a clear-sky day, the lake surface temperature

was measured by four TIR radiometers located around 38.69721 ° N and 118.70802 ° W. After correcting the effect of lake surface emissivity, the measured lake surface temperature is 290.56K (with a standard deviation of 0.07K in the four sets of measurements). The column water vapor calculated from the atmospheric profile measured by radiosonde is 0.95cm. Following the same procedures used in the Lake Titicaca vicarious field campaign (Wan et al., 2002), we estimated the calibration bias in the new A-side TIR data as shown in column 7 of Table 1. The root-sum-squares of uncertainties in the calibration accuracy estimate is about 0.3K for bands 20, 22-23, 29, and 31-32, and 0.8K for bands 21 and 33.

As shown in columns 4 and 5 of Table I, MODIS bands 31 and 32, which are used to retrieve LST with the generalized split-window algorithm, meet the NEDT specification. The effects of calibration bias in these two bands on the LST algorithm depend on the resulting errors in the average and difference of brightness temperatures in these two bands, i.e., errors in 0.5 $(T_{31} + T_{32})$ and 0.5 $(T_{31} - T_{32})$. The error in the first term caused by the calibration bias in both old and new A-side data is less than 0.1K. In the old A-side data, the error in the second term is around 0.3K, introducing an error of 0.5K or slightly larger to the retrieved LST. Although this amount of error is too large for SST to meet its accuracy specification of 0.3-0.5K, it is considered marginal for LST to meet the 1K accuracy specification. For the new A-side data, the error in the second term is much smaller. The estimated performance of bands 20, 22-23, 29, and 31-33, which are used in the MODIS day/night LST algorithm, shows that NEDT meets the specifications in all these bands, and that the calibration bias is small for longwave bands but is about 2-3% of the radiance in the three mid-wave bands for the old A-side data. For the new A-side data, the calibration bias is less than 1% in bands 22-23, 29, and 31-32.

5. MODIS LST PRODUCTS

5.1 A Brief Description

The MODIS LST data products are produced in a sequence. The sequence begins in a swath (scene) of MODIS data at a nominal pixel spatial resolution of 1km at nadir and a nominal swath coverage of 2030 or 2040 lines (along track, about five minutes of MODIS scans) by 1354 pixels per line. The first product, MOD11_L2, is a LST product at 1km spatial resolution for a swath. This product is the result of the generalized split-window LST algorithm (Wan and Dozier, 1996). The second product, MOD11A1, is a tile of daily LST product at 1km spatial resolution. It is generated by mapping the pixels from the MOD11_L2 products for a day to the Earth locations on the integerized sinusoidal projection. The third product, MOD11B1, is a tile of daily LST and emissivities at 5km spatial resolution. It is generated by the day/night LST algorithm (Wan and Li, 1997). The fourth product, MOD11A2, is an eight-day LST product by averaging the MOD11A1 product in a period of eight days. Other LST products are the daily, eight-day, and monthly global LST product in a geographic projection at the 0.25 ° spatial resolution of the Climate Modeling Grid (CMG) cells. They are derived from the MOD11A1 and MOD11B1 daily LST

products.

The level-2 LST product, MOD11_L2, is generated using the MODIS sensor radiance data product (MOD021KM), the geolocation product (MOD03), the cloud mask product (MOD35_L2), the atmospheric temperature and water vapor product (MOD07_L2), the quarterly landcover (MOD12Q1), and snow product (MOD10_L2). For complete global coverage, the MOD11_L2 LST product is generated for all swaths acquired in daytime and nighttime on the Earth including the polar regions. This MOD11_L2 LST product contains nine scientific data sets (SDSs): LST, QC for quality assurance (QA) control, Error_LST, Emis_31, Emis_32, View_angle, View_time, Latitude, and Longitude. The first seven DSDs are for 1km pixels. The last two DSDs are coarse resolution (5 km) latitude and longitude data. Each set corresponds to a center pixel of a block of 5 by 5 pixels in the LST SDS. For effective use of the space, the QC SDS uses 16 bits to store eight flags. Bits 00-01 are used for the Mandatory QA flags which is defined by the MODIS Land group: 00 stands for a pixel in which LST is produced in good quality, not necessary to examine more detailed QA bits; 01 for a pixel with LST produced in unreliable or unquantifiable quality, recommend examination of more detailed QA bits; 10 for a pixel not produced due to cloud effects (note that LST is produced only for pixels in clear-sky conditions at the 99% confidence); 11 for a pixel not produced primarily due to reasons other than cloud (for example, in ocean). Note that Fill Value 0 is not the fill value for the whole QC SDS. It is used only for the other seven flags. Therefore, the QC SDS should be used together with the LST SDS: for pixels with Fill Value 0 in the LST SDS, all the other seven flags in the QC SDS are given a fill value; the values in the other seven flags represent meaningful information related to the LST quality only for pixels with non-zero values (specifically, zero in the other seven flags means the best quality in LST).

The product generation executive (PGE) code for the daily MODIS LST products, PGE16, consists of two process segments: MOD_PR11A1 and MOD_PR11B1. The MOD_PR11A1 process generates LSTs in the MOD11_L2 product for all clear-sky pixels at a 99% confidence defined by MOD35_L2, and maps the LSTs to the 1km grids in the level-3 MOD11A1 product. The MOD_PR11A1 also accumulates all useful information into the interim products (MOD11UPD) in the 5km tiles, including radiance values in the seven bands used in the day/night LST algorithm which are contributed from clear-sky pixels, viewing angles and solar angles, and related information from the atmospheric profile. Based on the information in MOD11UPD, the MOD_PR11B1 process generates the LST and emissivity values with the day/night LST method at 5km resolution grids in the MOD11B1 product. Two new SDSs (LST_Day_5km_Aggregated_from_1km and LST_Night_5km_Aggregated_from_1km) are also included in the MOD11B1 product to store the LST values aggregated from the LST_Day_1km and LST_Night_1km data in the MOD11A1 product. These two SDSs have been used to produce the quick looks of the LST product in the MODIS Land Global Browse web page (http://modland.nascom.nasa.gov/browse).

5.2 A Double-Screen Scheme to Remove cloud-contaminated LSTs

Although the state-of-art techniques based on multiple MODIS bands have been used in the MODIS cloud mask product (MOD35_L2), and the MODIS LST PGE produces LSTs only for the clear-sky pixels at the highest confidence (99%) defined by MOD35_L2, there are still some small possibilities that MODIS LSTs are contaminated with cloud effects because of the difficulty to accurately discriminate true clear-sky pixels from cloud pixels and pixels contaminated with sub-pixel clouds. The quality assurance provided in the MODIS LST products at the pixel or grid levels is based on the quality information in the input products and the knowledge obtained from error analysis of LST algorithms in clear-sky conditions. Therefore, it is impossible to make the confidence of the quality assurance in the MODIS LST products higher than 99%.

The simulations of LST algorithms indicate that the difference in the LSTs retrieved by the day/night LST method and the LSTs retrieved by the generalized split-window LST method in clear-sky conditions depends on the uncertainties in the classification-based emissivities and the column water vapor, and it ranges from a few minus degrees K to 10K at most. But the range of difference calculated from the real MODIS LST products in large regions is sometimes much wide due to the different sensitivities of the two LST algorithms to the cloud effects. We propose the use of this LST difference statistics to remove the LST values that are contaminated with cloud effects: screening off 1% of both the daytime and nighttime LSTs by the upper and lower ends of the LST difference distributions. Figure 1 shows the histograms of the LST differences over the North America Continent between latitudes 20-50 ° on 21 July 2001. Figure 2 shows the images of daytime (a) and nighttime (b) LST differences, over the same region on the same day. In the color composite image in Figure 2(a), the red component represents the positive portion of the daytime LST difference in such a way that the grids screened off are at grey level of 255 and the remaining grids are in the grey scale of 15-215, the green component represents the negative portion of the daytime LST difference in a similar way, and the blue component is the LST difference itself in the grey scale of 15-255. Similarly for the nighttime LST difference in Figure 2(b). Therefore, the points in brightest red represent the grids screened off because their LST differences are too large in the negative direction, and points in the brightest green represent the grids screened off because their LST differences are too large in the negative direction. We can see that most of these screened grids in the brightest red and green are by the edges of the LST difference image (the blue component), i.e., they are close to the areas covered by clouds. Such a distribution of the screened grids justified this screen scheme proposed to remove the cloud-contaminated LSTs. Before the screening, the daytime LST difference ranges from -15K to 22K and the nighttime LST difference ranges from -26K to 35K. After the screening, the LST difference range reduces to -1.96 to 8.24K for the daytime and -3.36K to 6.84K for the nighttime. The averaged LST differences are 2.62K and 1.91K for the daytime and nighttime LSTs, respectively. The averaged LST differences are different because the daytime and nighttime LSTs are distributed in different areas and in the daytime LST image there are more clear-sky grids in the semi-arid and arid mid west regions where

surface emissivities have lower values. The difference between the LSTs retrieved from the day/night method and the LSTs retrieved from the split-window method reveals that the classification-based emissivities used in the split-window LST method are overestimated, especially in the semi-arid and arid regions. In the second step of the proposed double-screen scheme, the histogram of difference between daytime and nighttime LSTs is used to remove the grids contaminated with cloud effects after the first screen described above: screen off 0.5% of the daytime and nighttime LST pairs by the upper and lower ends of the LST difference distribution. Figure 3 shows the 5km daytime and nighttime LSTs, and the band emissivities in the 8-day period of July 20-27, 2001 for the same region as in Figure 2. In Figure 3(a), the red (R), green (G), and blue (B) components represent the histogram-enhanced daytime, nighttime LSTs and the day-night LST difference after screening out the cloud-contaminated grids with the double-screen scheme. In Figure 3(b), the RGB components represent the emissivities in MODIS bands 29, 22, and 20 enhanced with the histogram equalization method, respectively. The spatial features in the daytime and nighttime LSTs, the day-night LST, and the band emissivities show the great potentials of the 5km MODIS LST product in various applications. A complete coverage of the LST and surface emissivities can be obtained with more days of data.

6. VALIDATION RESULTS

The MODIS LST algorithms were validated with MAS data collected in several field campaigns since the field campaign conducted over a silt playa in Railroad Valley, Nevada, in June 1997 (Snyder et al., 1997a). According to the experience gained in our field campaigns, the major sources of uncertainties in the LST validation are the spatial variations in surface temperature and emissivity within a MAS or MODIS pixel. When these spatial variations are significantly large, it will not be possible to accurately measure the surface temperature at the scale of pixel size with ground-based instruments. The key requirements for a good site of LST validation are: its size being large enough to cover at least dozens of MODIS pixels, homogeneous surface materials and emissivity and temperature, its easy accessibility for the deployment of instruments, and less interference between the validation activities and the normal life activities.

In order to validate the MODIS LST product, we conducted three field campaigns in 2000 and four field campaigns in 2001 in California (CA) and Nevada (NV), in addition to the vicarious calibration field campaign conducted in Lake Titicaca, Bolivia in May/June 2000. The field campaigns conducted in 2000 include early April in Mono Lake and Bridgeport grassland in CA, late July in Railroad Valley NV, and in Mono Lake, Bridgeport grassland and a rice field in Chico, CA, and early October in Mono Lake and Bridgeport CA. The field campaigns conducted in 2001 include March-April in Bridgeport CA and Walker Lake NV, mid-late July in Railroad Valley NV, and in Mono Lake and Bridgeport CA, August in Mono Lake and Bridgeport CA, and October in Walker Lake NV and Bridgeport CA. Each field campaign lasted foe 2-3 weeks to cover a flight opportunity window of the MODIS Airborne Simulator (MAS).

6.1 Validation of the 1km Level 2 LST Product Using Lake Sites

We selected lake sites as our primary sites for LST validation in the first two years of MODIS LST production because of the following considerations. Because water surface emissivity can be accurately calculated from refractive index and surface temperature is often much more uniform in lakes than other land sites, lake surface radiometric temperature at a scale of 1km may be accurately measured by IR radiometers at multiple locations in most cases. We know that the uncertainty in surface emissivities in MODIS bands 31 and 32, and the residual error in LST after correcting the atmospheric effects with the split-window method are the only two major error sources in the level-2 1km MODIS LST product (MOD11_L2). We can reduce the emissivity-related error source to minimal with lakes as validation sites so that the residual error related to atmospheric corrections in the LST algorithm can be estimated by the difference between measured lake surface temperatures and the values in the MODIS LST product. If the surface temperature values in the MODIS LST product agree well with the measured lake surface temperatures in lake sites in different seasons, this will become evidence of the capability of the MODIS LST algorithm in atmospheric effect corrections. Once an estimate of the atmospheric-correction related residual error is obtained, we can apply this estimate to MODIS LST values in other locations, where it may be difficult or even impossible to make accurate in-situ measurements of surface temperatures at the 1km scale because of terrain and spatial variations in LST. In this way, we can indirectly validate the MODIS LST product in non-lake areas where the surface emissivities in bands 31 and 32 can also be well estimated from the land cover types and viewing angle, such as in vegetated areas. If we can make accurate ground-based measurements of lake surface temperature and atmospheric profile in dry atmospheric condition, the in situ measurement data can also be used to evaluate the calibration accuracy of MODIS TIR bands in the atmospheric windows. We selected Mono Lake and Waker Lake as our primary LST validation sites also because of the relative short distance between the sites and the UCSB campus and the distance between the sites and the aircraft base (Dryden Flight Research Center) for the MAS instrument so that we can arrange our field campaigns more flexibly and efficiently. We can drive to the sites from Santa Barbara with all ground-based instruments in two vehicles in a single day. It is possible to fly daytime and nighttime MAS missions in a single day when it is in good weather conditions. Mono Lake has a relatively large open water area in its eastern portion, approximately 13km in the S-N direction and 9km in the E-W direction. This portion will be covered by around 100 MODIS pixels. Lake Titicaca is a very good validation site for the TIR absolute radiances because it is a high elevation (3841m above sea level) lake located in a large plateau in South America and it has a large size of open water surface (8,100 km^2). The elevation of Mono Lake is 1945m above sea level. Walker Lake has a size of approximately 20km by 7km, at 1196m above sea level.

The same TIR radiometers and radiosonde system that were used in our vicarious calibration field campaign conducted in Lake Titicaca in June 2000 (Wan et al., 2002) were also used in our LST validation field campaigns. The detailed technical specifications and real performance qualities and the procedures to

correct the effect of surface emissivity on the measured surface temperature can be found in that MODIS calibration paper. The accuracy of the IR radiometers is better than 0.2K.

On April 4, 2000, a clear-sky day, four IR-radiometer floating systems were deployed in Mono Lake. The averaged value of lake surface kinetic temperatures measured by the IR radiometers at the MODIS overpass time is 283.81K with a standard deviation of 0.52K, as shown in columns 7 and 8 of case 1 in Table II. Note that each case occupied two lines. The averaged latitude and longitude values of the IR radiometers positions are given in column 3. Date and overpass time of the Terra MODIS are given in column 4. The zenith and azimuth angles of the MODIS observation are given in column 5. In column 6, the atmospheric column water vapor (cwv) in the upper line comes from MOD07_L2 and that in the lower line comes from radiosonde. Because we have only one radiosonde system, we cannot measure the atmospheric temperature and water vapor profile at each site when we make in situ measurements with IR radiometers in multiple sites at the same time. The version number of the MODIS level 1B data is given in column 9. The MODIS LST value, which in general is interpolated from the MOD11_L2 LST values at four pixels neighboring the averaged position of IR radiometers, is given in column 10. The difference between the MODIS LST value and the LST value from in situ measurements is given in the last column. In case 1, we cannot apply the 4-pixel interpolation because the positions of two IR radiometers are too close to Paoha island in the middle of the lake. Therefore, we shifted the averaged position to the east by 1km in this case only. The difference between the MODIS T_s value and the averaged in-situ measured lake surface temperature is 0.9K in this case. There are two reasons for this relatively large difference value: (1) MODIS level 1B data is in version 2.4.2 in this case so that the band 31 radiance has an error up to 0.5%; (2) The value of atmospheric column water vapor given by MOD07_L2 in its early version is 2.2cm, which is much larger than the value of 0.36cm calculated from the atmospheric humidity profile measured by radiosonde.

The next case is also for Mono Lake in the July field campaign. On July 25, we got good measurement data from only three IR radiometers and others had problems with the batteries. The IR radiometers were deployed far away from the lake shore. The averaged lake surface temperature measured by the IR radiometers is 296.01K with a standard deviation 0.15K. The MODIS LST calculated from MODIS L1B data in v2.5.4 is only 0.3K larger than the in situ value. Note that MODIS L1B data in version 2.5.4 or later give right radiance values in TIR bands (details are available in the version history file at the MODIS Calibration Support Team home page http://mcstweb.gsfc.nasa.gov/Home.html). In case 3, four IR radiometers were deployed all in the middle of the open water area on 6 October 2000. The MODIS LST value is larger than in the situ value by 0.2K.

Case 4 is for the field campaign conducted in Lake Titicaca, Bolivia on 15 June 2000. Five IR radiometers were deployed in this case. The MODIS LST value is larger than in the situ value by 0.5K. Details are given in Wan et al. (2002).

Case 5 is for the field campaign conducted in Walker Lake, Nevada on 18 October 2001. The MODIS LST value. which is retrieved from the new A-side MODIS data in v3.0.0, is larger than in the situ value by 0.2K.

As shown in the last column in the five cases of lake sites in Table II, the differences between LST values from the MODIS LST product and the in-situ measured LST values range from 0.2K to 0.9K. Except the first case in which there is a known error up to 0.5% in the MODIS band 31 data, the differences between MODIS and in situ LSTs are in the same level of the IR radiometer accuracy and the spatial variations in surface temperatures measured by IR radiometers and MODIS. The uncertainties related to the IR radiometer, spatial variations in the in-situ measured temperatures (i.e., the standard deviation divided by the square root of the total number of the IR radiometers) and in the MODIS measured temperature do not exceed 0.2K, 0.13K, and 0.5K, respectively. The root sum square (RRS) of all these three uncertainties is 0.55K. Therefore, we got the estimate of the residual error after atmospheric effect corrections in the 1km MODIS LST product, which is approximately 0.6K.

6.2 Validation of the 1km Level 2 LST Product Using Vegetation Sites

The same supporting structure used in the floating system for the IR radiometer was also used in the field campaign conducted in the Bridgeport grassland in early April 2000 just before the flood-irrigation started on 15 April, giving IFOV of 32cm in diameter on the grassland surface. Because there was no cattle and horse grazing on the grassland during the field campaign, we were allowed to deploy four IR radiometers in the middle of a grassland owned by Hunewill Circle H Ranch. The four IR radiometers were placed at the corners of a rectangle with a length of 50m each side with the hope that the measured surface temperatures can be compared to MAS data. Unfortunately, there was no MAS flight over the Mono Lake and Bridgeport area until October 2000 because of technical and schedule problems. At the beginning, one IR radiometer was intentionally deployed at a location where soil surface was more wet than other locations. The differences in the surface temperatures measured by the IR radiometers were up to 7K in daytime data and 5K in nighttime data around the MODIS overpass time. After we moved the IR radiometers into an area where grass was more uniform and there is no obvious difference in the soil surface moisture conditions, the maximum difference was still around 2K. The MODIS LST value is smaller than the in situ value by 0.9K. Because of the large variation in measured surface temperatures and the MODIS L1B data in v2.4.2, we should give less weight for this case (case 6).

Figure 4 shows the brightness temperature image calculated from band 45 radiance (centered at 10.95 μm) of MAS data collected over Bridgeport, CA on 6 October 2000. We can verify the large spatial variation in daytime LSTs with this MAS image by showing brightness temperature values of some MAS pixels (with the size of approximately 50m) by the location of our measurements: 305.7K at the pixel in line 362 sample 472 (latitude 38.225 °, longitude -119.268 °), 312.1K at the pixel in line 369 sample 468 (latitude 38.225 °, longitude -119.271 °), and 300.3K at the pixel in line 351 sample 465 (latitude 38.220 °, longitude

-119.268 °). The distance between the first two pixels is 403m and the third pixel is 652m away from the first pixel. These numbers show the difficulty for the in situ measurements of daytime LSTs and the great advantage of the thermal infrared remote sensing with MODIS in providing the global LST distribution at 1km resolution in clear-sky conditions in cases where it is difficult to make in situ measurements.

After the Bridgeport field campaign in April 2000, we designed a better strategy for measuring nighttime LST in grassland. During the late July field campaign, the Bridgeport grassland was irrigated, and there were cattle and horses grazing in the field. Instead of using the plastic supporting systems for the IR radiometers in the field, we set two poles by the edge of the grassland and fixed one IR radiometer at the top of each pole. The IR radiometer viewed toward the grassland surface at approximately 3.5m above ground, with IFOV of 1.5m in diameter. On the nights of July 27 and 29, two persons each carrying one IR radiometer walked forward and back along two almost parallel transects in the middle of the grassland under the clear-sky moon lights for more than one hour covering the MODIS nighttime overpass times. We averaged the measured surface temperatures along the transects and found that the averaged values are compatible to the values measured by the IR radiometers on the poles. The results for these two nights are listed as cases 7 and 8 in Table II.

During the late July field campaign, we also set one pole for an IR radiometer in the middle of a rice field in Chico, California, which is a test site used by Dr. Richard E. Plant, University of California at Davis. Because a series of rice fields with the size of approximately 50m by 50m each are distributed in the area, there are only narrow roads and irrigation canals between them, and there is no large difference between the surface temperatures over rice canopy and roads at night, we believe that the surface temperature measured by a single IR radiometer is still useful for the validation of nighttime MODIS LST product. The results for the rice field in the nights of July 27 and 29, 2000 are listed as cases 9 and 10 in Table II. From the five cases of LST validation using vegetation sites, we can see that the error in MODIS LSTs in dense vegetation areas is compatible to and slightly larger than the cases of lake sites.

As shown by the MODIS snow cover product in early March 2001, the Bridgeport grassland was fully covered by snow on March 11, a clear-sky day. The two IR radiometers gave almost identical surface temperature at the time of night overpass of Terra. The difference between the MODIS LST, which is retrieved from MODIS L1B data in v3.0.0, and the in situ measured LST is 0.2K as shown in case 11 of Table II. This is a good indication of the high quality of the MODIS TIR data in the B-side configuration.

6.3 Validation of the MODIS LST Product Using a Silt Playa in Railroad Valley, Nevada

In the last two sections, the 1km MODIS LSTs produced by the generalized split-window algorithm have been validated using lake sites and vegetation sites. We also conducted field campaigns over a silt playa in Railroad Valley, Nevada in July both in 2000 and 2001 in order to validate the MODIS LST products in semi-arid and arid regions where surface emissivities in bands 31 and 32 are more variable. The silt playa

has a size larger than 15km by 15km at elevation of 1410m above sea level. Figure 5 shows the brightness temperature image calculated from band 45 radiance of MAS data collected Railroad Valley on 23 June 1997. The brightness temperature varies a few degrees K in the central portion of the silt playa. As discussed in section 5.2, the classification-based surface emissivities in bands 31 and 32 are overestimated in semi-arid and arid regions so that the 1km MODIS LSTs retrieved by the split-window method would be underestimated. The 5km MODIS LSTs retrieved by the day/night LST method should be better in semi-arid and arid regions because the surface emissivities are also retrieved simultaneously with the LST.

Before evaluating the 1km and 5km MODIS LSTs, which are retrieved by two different methods, in semi-arid and arid regions, we compared them in some selected large sites with known surface emissivities. One of these sites is Lake Tahoe, California with a size of approximately 13km in the S-W direction and 28km in the N-S direction. Another site is Bridgeport when the grassland and its surroundings are fully covered by snow. As shown in the first case in Table III, the difference between the 1km and 5km MODIS LSTs over Lake Tahoe is less than 0.5K on 18 October 2001. On the same day, the calibration of MODIS TIR bands in the new A-side configuration has been validated in section 4 (see column 7 in Table I). Case 2 in Table III is for the snow-covered Bridgeport site, the difference between the 1km and 5km MODIS LSTs is 0.3K and the 5km MODIS LST is larger than the in situ measured LST by 0.5K. These two cases indicate that the 1km and 5km MODIS LSTs are within 0.5K over lake and snow sites where surface emissivities in bands 31 and 32 are known, and that the emissivities retrieved by the day/night method are underestimated by less than 0.01 approximately.

It will be ideal to find a large homogeneous site in semi-arid and arid areas so that we can accurately measure the surface temperature at the 5km grid scale to validate the 5km MODIS LST product. Unfortunately, we have not found such a site. So we take an alternative approach: measure the surface temperature at the 1km scale with multiple IR radiometers, aggregate the 1km MODIS LSTs retrieved by the split-window method to the 5km grids as used for the 5km MODIS LSTs retrieved by the day/night method, calculate the difference between the aggregated 1km LSTs and 5km LSTs at four 5km grids neighboring the in-situ measurement points, interpolate the difference at the average position of the IR radiometers, and then add the interpolated difference onto the 1km LST value to correct the effects associated with errors in the surface emissivities and atmospheric column water vapor used in the split-window method. Finally, we compare this corrected 1km MODIS LST (T_s^c) with the in-situ measured LSTs.

Cases 3-9 in Table III are the seven comparisons made for the MODIS LST products with the in situ measurement data that we collected over the silt playa in Railroad Valley, Nevada. Following the same procedures used in Wan et al. (2002), the emissivity effect on the LSTs measured by the IR radiometers is calculated based on the spectral emissivity averaged from our measurements of silt playa samples collected from the site, typical atmospheric temperature and water vapor profiles measured at the site, and

the spectral response function of the IR radiometer. It is 1.95K with an estimated uncertainty slightly less than 1K due to the spatial variation in the surface emissivities. Figure 6 shows the playa surface temperatures measured by seven radiometers in Railroad Valley, NV on 21 July 2001. The solid, dashed, and dotted lines represent the surface temperatures measured by three IR radiometers located at corners of a rectangle of 100m by 100m. The four symbols represent the surface temperatures measured by four IR radiometers located at the center of the rectangle. In order to measure the viewing angle effect, these four IR radiometers were placed in a box in a such way that they viewed the same portion on the surface at a zenith angle of 15 degree from nadir and in the four azimuth directions of E, S, W, and N. In this case, there were significant temporal variations in the measured LSTs before noon, the spatial variations were about 1K, and the viewing angle effect was less than 0.3K. Fortunately, the temporal variation was smaller around the time of Terra overpass. In Table III, columns 1-8 are similar to those in Table II, column 9 is for the 1km MODIS LST, and column 10 is for T_s^c (the 1km MODIS LST after the correction with the 5km MODIS LST), and column 11 is for the difference between T_s^c and the in situ measured LSTs. If we compare the values in columns 7 and 9 for cases 3-9, we find that the 1km MODIS LSTs retrieved by the split-window method are underestimated by -1.3K to -2.7K at different viewing angles under different atmospheric conditions. After the correction with the 5km MODIS LSTs retrieved by the day/night method, the differences reduce to the range from -0.6K to 0.7K in the seven cases. We consider the Bridgeport snowcover case (case 2 in Table III) as a direct validation and these seven Railroad Valley cases as indirect validations of the 5km MODIS LST product.

6.3 Summary of the Validation Results

All the validation results in Tables II and III are presented in Figure 7 in order to show the range of LSTs in the validations. The height of the vertical dashed line at each data point represents the uncertainty in the in situ LST value. The error associated with the uncertainty in surface emissivities is 0.2K, 0.5K, and 0.9K for lake, grassland/snowcover/rice field, and silt playa sites, respectively. In summary, the MODIS LST products were validated in 19 cases in the LST range from 263K to 322K and the atmospheric column water vapor range from 0.4 to 3.0cm.

7. CONCLUSION

A double-screen scheme based on the difference between the 5km LST retrieved by the day/night LST algorithm and the aggregated 1km LST retrived by the generalized split-window algorithm, and the difference between daytime and nighttime LSTs, is proposed to remove the LSTs contaminated with cloud effects. The accuracy of daily MODIS LST product at 1km resolution, which was produced by the generalized split-window algorithm, was validated in eleven clear-sky cases with in-situ measurement data collected in field campaigns in 2000 and 2001. The MODIS LST accuracy is better than 1K in the range from 263K to 300K over Lake Titicaca in Bolivia, Mono Lake, Bridgeport grassland, and a rice field in

Chico, California, and Walker Lake, Nevada, in the atmospheric column water vapor range from 0.4 to 3.0cm. In seven cases over a silt playa in Railroad Valley, Nevada, the 1km MODIS LSTs are a few Kelvin degrees lower than the in-situ measured LSTs because the surface emissivities inferred from land cover types in the split-window LST method are often overestimated in semi-arid and arid regions. After a correction with the difference between the 5km LST retrieved by the day/night LST method and the LST aggregated from 1km LSTs retrieved by the split-window method, the MODIS LSTs agree with in-situ measured LSTs within ±1K in the range from 263K to 322K for the seven cases in Railroad Valley and one case of snowcover in Bridgeport, California. It is recommended that the 1km LST product retrieved by the generalized split-window LST method be used for lakes, snow/ice, and dense vegetated areas, and the 5km LST product retrieved by the day/night LST method be used in bare and sparse vegetated areas.

Acknowledgment

This work was supported by EOS Program contract NAS5-31370 of the National Aeronautics and Space Administration. The field campaign activities conducted in Bridgeport, California, were partly supported by NASA grant NAG13-99023, in which Dr. Kenneth W. Tate, University of California at Davis is PI, and Dr. Zhengming Wan is co-PI. The authors would like to thank Dr. Robert Jellison, University of California/Sierra Nevada Aquatic Research Lab., Dr. Richard E. Plant, University of California at Davis, Mr. Stan Hunewill and Jeff Hunewill, Hunewill Guest Ranch, Bridgeport, California, for their supports in the LST validation activities. The MODIS data were generated by the Goddard DAAC under supports of MODIS MCST and SDDT. The MODIS LST product was generated by the MODAPS under supports of MODIS SDDT, its routine quality assessment was performed by the LDOPE, and the LST product was distributed by the EDC DAAC. The authors would like to thank John C. Price and other two anonymous reviewers for their valuable comments and suggestions, which helped to improve the paper.

REFERENCES

Becker, F., ‘‘The impact of spectral emissivity on the measurement of land surface temperature from a satellite,’’ *Int. J. Remote Sens.*, vol. 8, no. 10, pp. 1509-1522, 1987.

Becker, F. and Z.-L. Li, ‘‘Toward a local split window method over land surface,’’ *Int. J. Remote Sens.*, vol. 11, no. 3, pp. 369-393, 1990.

Berk, A., G. P. Anderson, L. S. Bernstein, P. K. Acharya, H. Dothe, M. W. Matthew, S. M. Adler-Golden, J. H. Chetwynd, Jr., S. C. Richtmeier, B. Pukall, C. L. Allred, L. S. Jeong, and M. L. Hoke, ‘‘MODTRAN4 radiative transfer modeling for atmospheric correction,’’ *Optical Spectroscopic Techniques and Instrumentation for Atmospheric and Space Research III, Proc. SPIE*, vol. 3756, pp. 348-353, 1999.

Brown, O. B., R. H. Evans, and P. Cornillon, ‘‘Satellite-derived global sea surface temperature fields: 1982-1989,’’ *Global and Planetary Change*, vol. 90, pp. 179-181, 1991.

Bruegge, C. J., J. E. Conel, R. O. Green, J. S. Margolis, R. G. Holm, and G. Toon, ‘‘Water vapor column abundance retrievals during FIFE,’’ *J. Geophys. Res.*, vol. 97, no. D17, pp. 18759-18768, 1992.

Brutsaert, W., A. Y. Hsu, and T. J. Schmugge, ‘‘Parameterization of surface heat fluxes above forest with satellite thermal sensing and boundary-layer soundings,’’ *J. Appl. Meteor.*, vol. 32, no. 5, pp. 909-917, 1993.

Caselles, V. and J. A. Sobrino, ‘‘Determination of frosts in orange groves from NOAA-9 AVHRR data,’’ *Remote Sens. Environ.*, vol. 29, no. 2, pp. 135-146, 1989.

Chedin, A., M. A. Scott, C. Wahiche, and P. Moulinier, ‘‘The improved initialization inversion method: a high resolution physical method for temperature retrievals from the Trios-N series,’’ *J. Clim. Appl. Meteorol.*, vol. 24, pp. 124-143, 1985.

Diak, G. R. and M. S. Whipple, ‘‘Improvements to models and methods for evaluating the land-surface energy balance and effective roughness using radiosonde reports and satellite-measured skin temperature data,’’ *Agricul. and Forest Meteorol.*, vol. 63, no. 3-4, pp. 189-218, 1993.

Ehrlich, D. and E. F. Lambin, ‘‘The surface temperature-vegetation index space for land cover and land-cover change analysis,’’ *Int. J. Remote Sens.*, vol. 17, no. 3, pp. 463-487, 1996.

Esaias, W. E., M. R. Abbott, I. Barton, O. W. Brown, J. W. Campbell, K. L. Carder, D. K. Clark, R. L. Evans, F. E. Hoge, H. R. Gordon, W. P. Balch, R. Letelier, and P. J. Minnett, ‘‘An overview of MODIS capabilities for ocean science observations,’’ *IEEE Trans. Geosci. Remote Sens.*, vol. 36, no. 4, pp. 1250-1265, 1998.

Feldhake, C. M., D. M. Glenn, and D. L. Peterson, ‘‘Pasture soil surface temperature response to drought,’’ *Agron. J.*, vol. 88, no. 4, pp. 652-656, 1996.

French, A. N., T. J. Schmugge, and W. P. Kustas, ‘‘Discrimination of senescent vegetation using thermal emissivity contrast,’’ *Remote Sens. Environ.*, vol. 74, no. 2, pp. 249-254, 2000a.

French, A. N., T. J. Schmugge, and W. P. Kustas, ‘‘Estimating surface fluxes over the SGP site with remotely sensed data,’’ *Physics and Chemistry of the Earth Part B - Hydrology Oceans and Atmosphere*, vol. 25, no. 2, pp. 167-172, 2000b.

Fuchs, M. and C. B. Tanner, ‘‘Infrared thermometry of vegetation,’’ *Agron. J.*, vol. 58, pp. 597-601, 1966.

Gao, B. C. and Y. J. Kaufman, ‘‘Selection of the 1.375μm MODIS channel for remote sensing of cirrus cloud and stratospheric aerosols from space,’’ *J. Atmos. Sci.*, vol. 52, no. 23, pp. 4231-4237, 1995.

Gillespie, A., ‘‘Lithologic mapping of silicate rocks using TIMS,’’ in *TIMS Data Users’ Workshop*, pp. 29-44, Pasadena, CA: Jet Propul. Lab., JPL Publication 86-38, 1985.

Gillespie, A. R., S. Rokugawa, T. Matsunaga, J. S. Cothern, S. Hook, and A. B. Kahle, ‘‘A temperature and emissivity separation algorithm for Advanced Spaceborne Thermal Emission and Reflection Radiometer (ASTER) images,’’ *IEEE Trans. Geosci. Remote Sens.*, vol. 36, pp. 1113-1126, 1998.

Jackson, R. D., R. J. Reginato, and S. B. Idso, ‘‘Wheat canopy temperature: a practical tool for evaluating water requirements,’’ *Water Resour. Res.*, vol. 13, pp. 651-656, 1977.

Jin, M. J. and R. E. Dickinson, ‘‘Interpolation of surface radiative temperature measured from polar orbiting satellites to a diurnal cycle - 1. without clouds,’’ *J. Geophys. Res.*, vol. 104, no. ND2, pp. 2105-2116, 1999.

Justice, C. O., E. Vermote, J. R. G. Townshend, R. Defries, D. O. Roy, D. K. Hall, V. V. Salomonson, J. L. Privette, G. Riggs, A. Strahler, W. Lucht, R. B. Myneni, K. Knyazikhin, S. W. Running, P. R. Nemani, Z. Wan, A. R. Huete, W. van Leeuwen, R. E. Wolfe, L. Giglio, J.-P. Muller, and Y. Knyazikhin, M. J. Barnsley, ‘‘The Moderate Resolution Imaging Spectroradiometer (MODIS): land remote sensing for global change research,’’ *IEEE Trans. Geosci. Remote Sens.*, vol. 36, pp. 1228-1249, 1998.

Kahle, A. B., D. P. Madura, and J. M. Soha, ‘‘Middle infrared multispectral aircraft scanner data: analysis for geological applications,,’’ *Appl. Optics*, vol. 19, pp. 2279-2290, 1980.

Kaufman, Y. J., C. O. Justice, L. P. Flynn, L. D. Kendall, E. M. Prins, L. Giglo, D. E. Ward, W. P. Menzel, and A. W. Setzer, ‘‘Potential global fire monitoring from EOS-MODIS,’’ *J. Geophys. Res.*, vol. 103, no. D24, pp. 32215-32238, 1998.

Kealy, P. S. and A. R. Gabell, ‘‘Estimation of emissivity and temperature using alpha coefficients,’’ in *Proc. 2nd TIMS Workshop*, pp. 11-15, Pasadena, CA: Jet Propul. Lab., JPL Publication 90-55, 1990.

Kerr, Y. H., J. P. Lagouarde, and J. Imbernon, ‘‘Accurate land surface temperature retrieval from AVHRR data with use of an improved split window algorithm,’’ *Remote Sens. Environ.*, vol. 41, no. 2-3, pp. 197-209, 1992.

King, M. D., Y. J. Kaufman, W. P. Menzel, and D. Tanré, ‘‘Remote sensing of cloud, aerosol, and water vapor properties from the Moderate Resolution Imaging Spectrometer (MODIS),’’ *IEEE Trans. Geosci. Remote Sens.*, vol. 30, no. 1, pp. 2-27, 1992.

Lambin, E. F. and D. Ehrlich, ‘‘Land-cover changes in sub-Saharan Africa (1982-1991): Application of a change index based on remotely sensed surface temperature and vegetation indices at a continental scale,’’ *Remote Sens. Environ.*, vol. 61, no. 2, pp. 181-200, 1997.

Li, Z.-L. and F. Becker, ‘‘Feasibility of land surface temperature and emissivity determination from AVHRR data,’’ *Remote Sens. Environ.*, vol. 43, pp. 67-85, 1993.

Li, Z.-L., F. Becker, M. P. Stoll, and Z. Wan, ‘‘Evaluation of six methods for extracting relative emissivity spectra from thermal infrared images,’’ *Remote Sens. Environ.*, vol. 69, pp. 197-214, 1999.

Ma, X., Z. Wan, C. C. Moeller, W. P. Menzel, L. E. Gumley, and Y. Zhang, ‘‘Retrieval of geophysical parameters from Moderate Resolution Imaging Spectroradiometer thermal infrared data: evaluation of a two-step physical algorithm,’’ *Appl. Optics*, vol. 39, no. 20, pp. 3537-3550, 2000.

Ma, X.-L., Z. Wan, C. C. Moeller, W. P. Menzel, and L. E. Gumley, ‘‘Simultaneous retrieval of atmospheric profiles and land-surface temperature/emissivity from Moderate Resolution Imaging Spectroradiometer thermal infrared data: extension of a two-step physical algorithm,’’ *Appl. Optics*,

in press 2002.

Mannstein, H., ''Surface energy budget, surface temperature and thermal inertia,'' in *Remote Sensing Applications in Meteorology and Climatology*, ed. R. A. Vaughan and D. Reidel, NATO ASI Ser. C: Math. Phys. Sci. Vol. 201, pp. 391-410, Dordrecht, Netherlands: A Reidel Publishing Co., 1987.

McVicar, T. R. and D. L. B. Jupp, ''The current and potential operational uses of remote sensing to aid decisions on drought exceptional circumstances in Australia: a review,'' *Agricultural Systems*, vol. 57, no. 3, pp. 399-468, 1998.

Muchoney, D. M., J. S. Borak, H. Chi, M. Friedl, J. Hodges, N. Morrow, and A. Strahler, ''Application of the MODIS global supervised classification model to vegetation and land cover mapping of Central America,'' *Int. J. Remote Sens.*, vol. 21, no. 6/7, pp. 1115-1138, 1999.

Nerry, F., F. Petitcolin, and M. P. Stoll, ''Bidirectional reflectivity in AVHRR channel 3: application to a region in Northern Africa,'' *Remote Sens. Environ.*, vol. 66, pp. 298-316, 1998.

Ottlé, C. and M. Stoll, ''Effect of atmospheric absorption and surface emissivity on the determination of land temperature from infrared satellite data,'' *Int. J. Remote Sens.*, vol. 14, no. 10, pp. 2025-2037, 1993.

Ottlé, C. and D. Vidal-Madjar, ''Estimation of land surface temperature with NOAA9 data,'' *Remote Sens. Environ.*, vol. 40, no. 1, pp. 27-41, 1992.

Padilla, H. G., A. C. Leyva, and P. A. Mosino, ''An analysis of daily humidity patterns at a mountainous and urban site in a tropical high-altitude region,'' *J. Appl. Meteorol.*, vol. 32, pp. 1638-1646, 1993.

Plokhenko, Y. and W. P. Menzel, ''The effects of surface reflection on estimating the vertical temperature-humidity distribution from spectral infrared measurements,'' *J. Appl. Meteorol.*, vol. 39, pp. 3-14, 2000.

Prata, A. J., ''Land surface temperatures derived from the advanced very high resolution radiometer and the along-track scanning radiometer 2. experimental results and validation of AVHRR algorithms,'' *J. Geophys. Res.*, vol. 99, no. D6, pp. 13025-13058, 1994.

Price, J. C., ''Estimating surface temperature from satellite thermal infrared data - a simple formulation for the atmospheric effect,'' *Remote Sens. Environ.*, vol. 13, pp. 353-361, 1983.

Price, J. C., ''Land surface temperature measurements from the split window channels of the NOAA-7 AVHRR,'' *J. Geophys. Res.*, vol. 79, pp. 5039-5044, 1984.

Price, J. C., ''On the use of satellite data to infer surface fluxes at meteorological scales,'' *J. Appl. Meteor.*, vol. 21, pp. 1111-1122, 1982.

Realmuto, V. J., ''Separating the effects of temperature and emissivity: emissivity spectrum normalization,'' in *Proc. 2nd TIMS Workshop*, pp. 23-27, Pasadena, CA: Jet Propul. Lab., JPL Publication 90-55, 1990.

Salomonson, V., W. Barnes, P. Maymon, H. Montgomery, and H. Ostrow, ''MODIS: advanced facility instrument for studies of the Earth as a system,'' *IEEE Trans. Geosci. Remote Sens.*, vol. 27, no. 2, pp. 145-153, 1989.

Sellers, P. J., F. G. Hall, G. Asrar, D. E. Strebel, and R. E. Murphy, ''The first ISLSCP Field Experiment (FIFE),'' *Bull. Amer. Meteorol. Soc.*, vol. 69, no. 1, pp. 22-27, 1988.

Smith, T. M. and R. W. Reynolds, ''A high-resolution global sea surface temperature climatology for the 1961-90 base period,'' *J. Climate*, vol. 11, pp. 3320-3323, 1998.

Smith, W. L., H. M. Woolf, and A. J. Schriener, ‘‘Simultaneous retrieval of surface and atmospheric parameters: a physical and analytically direct approach,’’ in *Advances in Remote Sensing Retrieval Methods*, ed. A. Deepak, H. E. Fleming, and M. T. Chahine, pp. 221-232, Hampton, Va., USA: A. Deepak Publishing, 1985.

Snyder, W. and Z. Wan, ‘‘BRDF models to predict spectral reflectance and emissivity in the thermal infrared,’’ *IEEE Trans. Geosci. Remote Sens.*, vol. 36, no. 1, pp. 214-225, 1998.

Snyder, W., Z. Wan, Y. Zhang, and Y.-Z. Feng, ‘‘Requirements for satellite land surface temperature validation using a silt playa,’’ *Remote Sens. Environ.*, vol. 61, no. 2, pp. 279-289, 1997a.

Snyder, W., Z. Wan, Y. Zhang, and Y.-Z. Feng, ‘‘Thermal infrared (3-14 μm) bidirectional reflectance measurements of sands and soils,’’ *Remote Sens. Environ.*, vol. 60, pp. 101-109, 1997b.

Snyder, W. C., Z. Wan, Y. Zhang, and Y.-Z. Feng, ‘‘Classification-based emissivity for land surface temperature measurement from space,’’ *Int. J. Remote Sens.*, vol. 19, no. 14, pp. 2753-2774, 1998.

Sobrino, J. A., C. Coll, and V. Caselles, ‘‘Atmospheric corrections for land surface temperature using AVHRR channel 4 and 5,’’ *Remote Sens. Environ.*, vol. 38, no. 1, pp. 19-34, 1991.

Susskind, J., J. Rosenfield, D. Reuter, and M. T. Chahine, ‘‘Remote Sensing of weather and climate parameters from HIRS2/MSU on TIROS-N,’’ *J. Geophys. Res.*, vol. 89, no. D3, pp. 4677-4697, 1984.

Townshend, J. R. G., C. O. Justice, D. Skole, J.-P. Malingreau, J. Cihlar, P. Teillet, and S. Ruthenberg, ‘‘The 1km resolution global data set: needs of the International Geosphere Biosphere Programme,’’ *Int. J. Remote Sens.*, vol. 15, pp. 3417-3441, 1994.

Vidal, A., ‘‘Atmospheric and emissivity correction of land surface temperature measured from satellite using ground measurements or satellite data,’’ *Int. J. Remote Sens.*, vol. 12, no. 12, pp. 2449-2460, 1991.

Wan, Z. and J. Dozier, ‘‘A generalized split-window algorithm for retrieving land-surface temperature from space,’’ *IEEE Trans. Geosci. Remote Sens.*, vol. 34, no. 4, pp. 892-905, 1996.

Wan, Z. and J. Dozier, ‘‘Land-surface temperature measurement from space: physical principles and inverse modeling,’’ *IEEE Trans. Geosci. Remote Sens.*, vol. 27, no. 3, pp. 268-278, 1989.

Wan, Z., ‘‘Estimate of noise and systematic error in early thermal infrared data of the Moderate Resolution Imaging Spectroradiometer (MODIS),’’ *Remote Sens. Environ.*, vol. 80, no. 1, pp. 47-54, 2002.

Wan, Z. and Z.-L. Li, ‘‘A physics-based algorithm for retrieving land-surface emissivity and temperature from EOS/MODIS data,’’ *IEEE Trans. Geosci. Remote Sens.*, vol. 35, no. 4, pp. 980-996, 1997.

Wan, Z., Y. Zhang, Z.-L. Li, R. Wang, V. V. Salomonson, A. Yves, and R. Bosseno, ‘‘Preliminary estimate of calibration of the Moderate Resolution Imaging Spectroradiometer (MODIS) thermal infrared data using Lake Titicaca,’’ *Remote Sens. Environ.*, in press 2002.

Watson, K., ‘‘Spectral ratio method for measuring emissivity,’’ *Remote Sens. Environ.*, vol. 42, pp. 113-116, 1992.

TABLE I. Specifications of the Terra MODIS TIR bands, and its estimated performance in the A-side configuration before 31 October 2000 (Wan et al., 2002) and the new A-side configuration after 3 July 2001.

band	bandwidth (μm)	IFOV	NEDT specified (K)	NEDT (K) estimated (Wan, 2002)	calibration bias estimated (K) (before 2000/10/31)	calibration bias estimated (K) (after 2001/07/03)
20	3.660-3.840	1km	0.05	0.06	0.60	0.63
21	3.929-3.989	1km	2.00	0.64	0.46	0.70
22	3.929-3.989	1km	0.07	0.07	0.55	0.15
23	4.020-4.080	1km	0.07	0.05	0.40	-0.18
24	4.433-4.498	1km	0.25	0.13		
25	4.482-4.549	1km	0.25	0.08		
27	6.535-6.895	1km	0.25	0.12		
28	7.175-7.475	1km	0.25	0.09		
29	8.400-8.700	1km	0.05	0.03	0.03	-0.12
30	9.580-9.880	1km	0.25	0.08		
31	10.780-11.280	1km	0.05	0.03	0.12	0.09
32	11.770-12.270	1km	0.05	0.05	-0.19	0.05
33	13.185-13.485	1km	0.25	0.16	0.55	(0.98)
34	13.485-13.785	1km	0.25	0.27		
35	13.785-14.085	1km	0.25	0.23		
36	14.085-14.385	1km	0.35	0.41		

TABLE II. Comparison between the 1km MODIS LSTs and in-situ measured LSTs in validation field campaigns conducted in 2000 and 2001. Note that each case occupied two lines. The atmospheric column water vapor (cwv) in the upper line comes from MOD07_L2 and that in the lower line comes from radiosonde. Most MOD11_L2 LSTs are retrieved from L1B data in version 2.5.4 or later except cases 1, 3 and 6.

case no.	site	latitude longitude (°)	date (m/d/y) time	view zenith azimuth (°)	atmos. cwv (cm)	in situ T_s from radiometers (K) (no.)	spatial variation δT_s (K)	MODIS L1B version	MODIS T_s (δT_s) (K)	MODIS - in situ T_s (K)
1	Mono Lake California	37.9712N 119.0014W	4/04/00 11:19 PST	22.38 -78.35	2.2 (0.36)	283.81 (4)	0.52	2.4.2	284.7 (0.2)	+0.9
2	Mono Lake California	37.9930N 118.9646W	7/25/00 11:18 PST	22.09 -79.37	2.1	296.01 (3)	0.15	2.5.4	296.3 (0.2)	+0.3
3	Mono Lake California	38.0105N 118.9695W	10/06/00 11:11 PST	11.35 -78.19	1.4 (0.62)	290.17 (4)	0.23	2.4.3	290.4 (0.1)	+0.2
4	Lake Titicaca Bolivia	16.2470S 68.7230W	6/15/00 15:26 UTC	34.3 -82.7	1.1 (0.29)	285.0 (5)	0.3	2.5.4	285.5 (0.5)	+0.5
5	Walker Lake Nevada	38.6972N 118.70802W	10/18/01 10:57 PST	0.74 -100.23	0.81 (0.95)	290.56 (4)	0.1	3.0.0	290.74 (0.2)	+0.2
6	Bridgeport California	38.2255N 119.2680W	4/04/00 11:19 PST	20.00 -79.38	2.6	308.2 (4)	0.9	2.4.2	307.3 (2.3)	-0.9
7	Bridgeport grassland	38.2202N 119.2693W	7/27/00 22:09 PST	11.81 81.33	1.6	281.63 (4)	0.6	2.5.4	282.4 (0.4)	+0.8
8	Bridgeport grassland	38.2202N 119.2693W	7/29/00 21:57 PST	32.36 77.56	2.4	283.24 (4)	0.6	2.5.4	283.0 (0.2)	-0.2
9	rice field California	39.5073N 121.8107W	7/27/00 22:10 PST	26.1 77.3	1.4	291.20 (1)		2.5.4	292.1 (0.5)	+0.9
10	rice field California	39.5073N 121.8107W	7/29/00 21:57 PST	42.67 75.8	3.0	293.02 (1)		2.5.4	292.9 (0.8)	-0.1
11	Bridgeport snowcover	38.2199N 119.2683W	3/11/01 22:36 PST	40.48 -97.32	0.4	263.50 (2)	(0.2)	3.0.0	263.7 (0.2)	+0.2

TABLE III. The difference between the 5km LST retrieved by the day/night LST method and the LST aggregated from 1km LSTs retrieved by the generalized split-window method. This difference is used to correct the effects associated with errors in the surface emissivities and atmospheric column water vapor used in the split-window method. Thus corrected MODIS LST (T_s^c) values are compared with the in-situ measured LSTs in the validation field campaigns conducted in 2000 and 2001.

case no.	site	latitude longitude (°)	date (m/d/y) time	view zenith azimuth (°)	atmos. cwv (cm)	in situ T_s from radiometers (K) (no.)	spatial variation δT_s (K)	MODIS T_s (δT_s) (K)	MODIS T_s^c (K)	T_s^c - in situ T_s (K)
1	Lake Tahoe California	39.171N 120.104W	10/18/01 10:57 PST	40.48 -97.32	0.4			289.12	289.60	
2	Bridgeport snowcover	38.2199N 119.2683W	3/11/01 22:36 PST	40.48 -97.32	0.4	263.5 (2)	(0.2)	263.7 (0.2)	264.0	+0.5
3	Railroad Valley, NV	38.4614N 115.6914W	7/27/00 22:09 PST	15.68 -98.85	0.77 (1.04)	289.9 (2)	(0.3)	288.7 (0.1)	289.3	-0.6 [A]
4	Railroad Valley, NV	38.4617N 115.6927W	7/18/01 10:35 PST	22.25 99.48	1.25 (0.86)	321.2 (3)	0.8	318.5 (0.7)	321.3	+0.1
5	Railroad Valley, NV	38.4617N 115.6925W	7/19/01 11:17 PST	47.36 -75.12	1.12	321.3 (3)	2.7	319.2 (0.5)	322.0	+0.7
6	Railroad Valley, NV	38.4617N 115.6926W	7/19/01 22:21 PST	43.78 -96.05	0.64	287.4 (3)	0.3	286.1 (0.4)	287.4	+0.0
7	Railroad Valley, NV	38.4617N 115.6926W	7/20/01 21:26 PST	44.40 75.49	0.69	289.7 (4)	0.3	287.5 (0.2)	289.6	-0.1
8	Railroad Valley, NV	38.4630N 115.6930W	7/21/01 11:05 PST	32.54 -77.26	0.68 (0.92)	320.1 (7)	0.4	317.7 (0.4)	319.8	-0.3
9	Railroad Valley, NV	38.4630N 115.6930W	7/23/01 21:57 PST	5.0 -98.04	1.01	290.7 (4)	0.5	288.8 (0.6)	290.6	-0.1

Note [A]: the L1B data is in version 2.5.4 but the MOD07_L2 data is based on L1B data in version 2.4.2 in case 3.

Figure Captions

Fig. 1, Histograms of the difference between the 5km and 1km LSTs over the North America Continent between latitudes 20-50° on 21 July 2001.

Fig. 2, Color composite images of daytime (a) and nighttime (b) LST differences over the same region on the same day as in Figure 1. See text for details of the RGB components.

Fig. 3, Color composite images of the 5km daytime and nighttime LSTs and their difference (a), and the band emissivities (b) in the 8-day period of July 20-27, 2001 for the same region as in Figure 2.

Fig. 4, Brightness temperature image calculated from band 45 radiance (centered at 10.95μm) of MAS data collected over Bridgeport, CA on 6 October 2000.

Fig. 5, Brightness temperature image calculated from band 45 radiance (centered at 10.95μm) of MAS data collected over Railroad Valley, NV on 23 June 1997.

Fig. 6, Surface temperatures measured by seven radiometers in Railroad Valley, NV on 21 July 2001.

Fig. 7, Comparison between the MODIS LSTs and the LSTs from in-situ measurements.

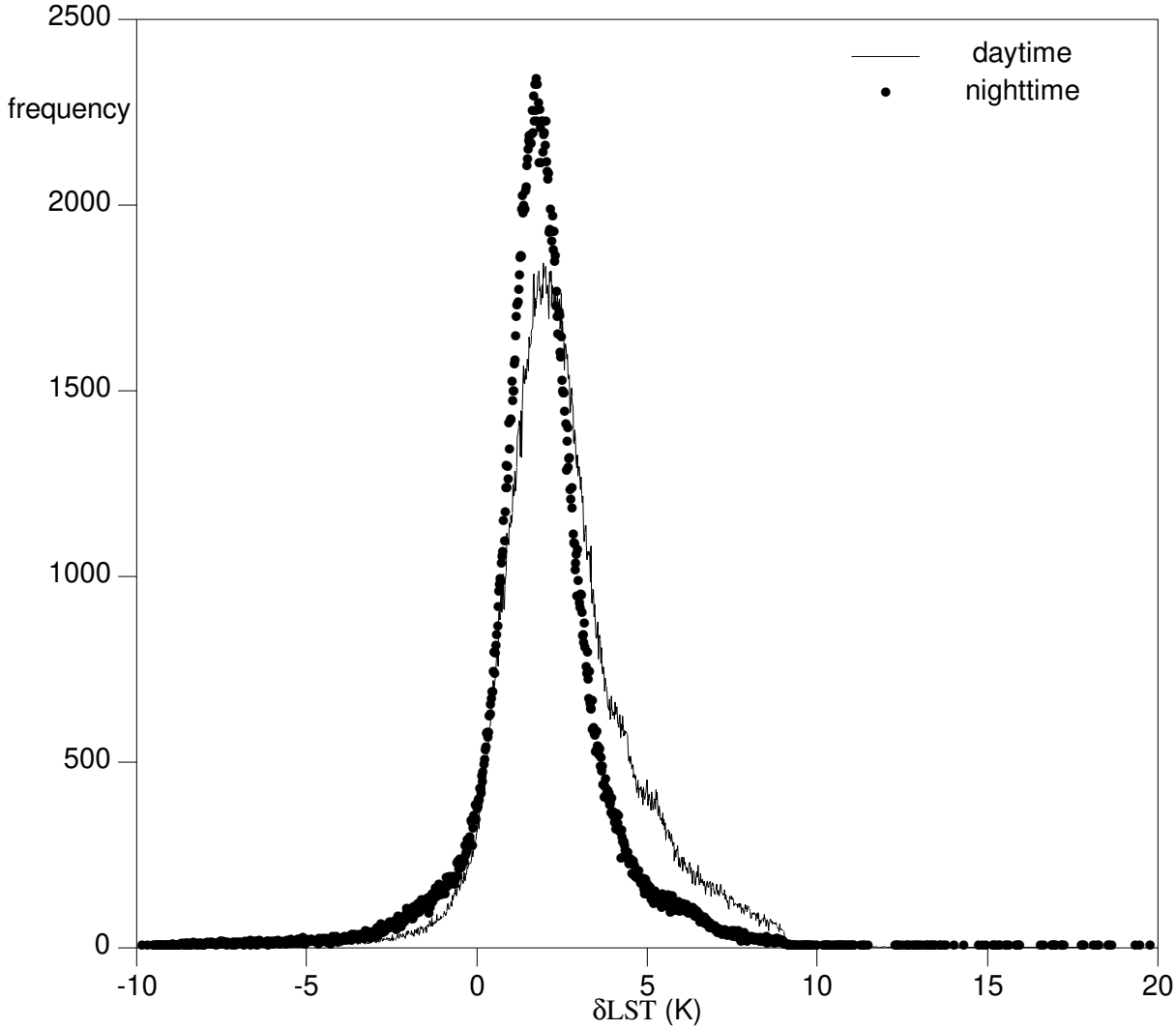

Fig. 1, Histgram of the difference between the 5km and 1km LSTs over the North America Continent between latitudes 20-50° on 21 July 2001.

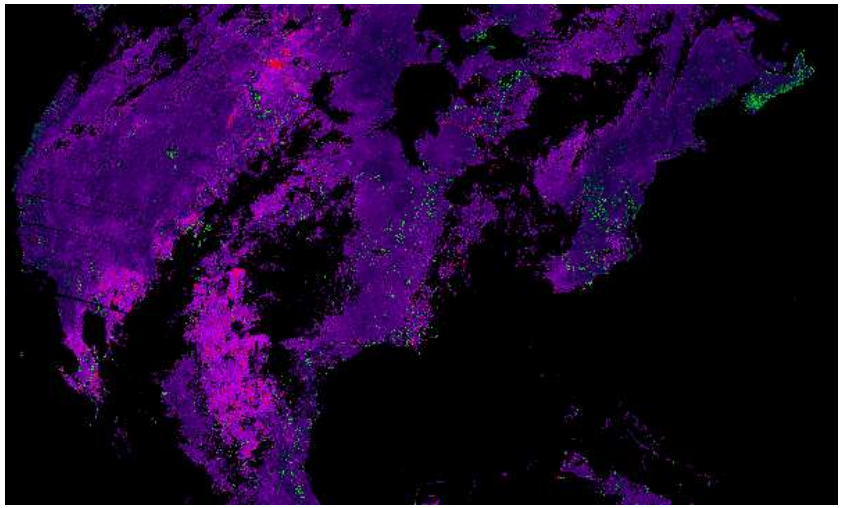

Fig. 2(a)

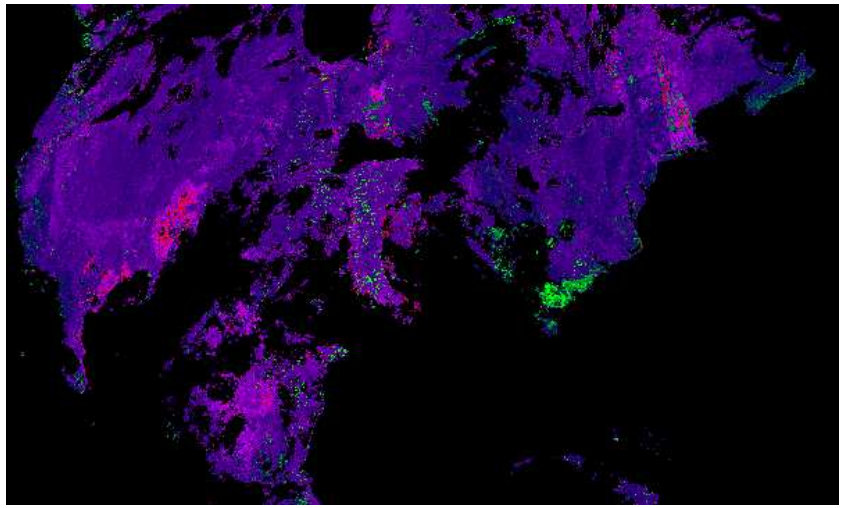

Fig. 2(b)

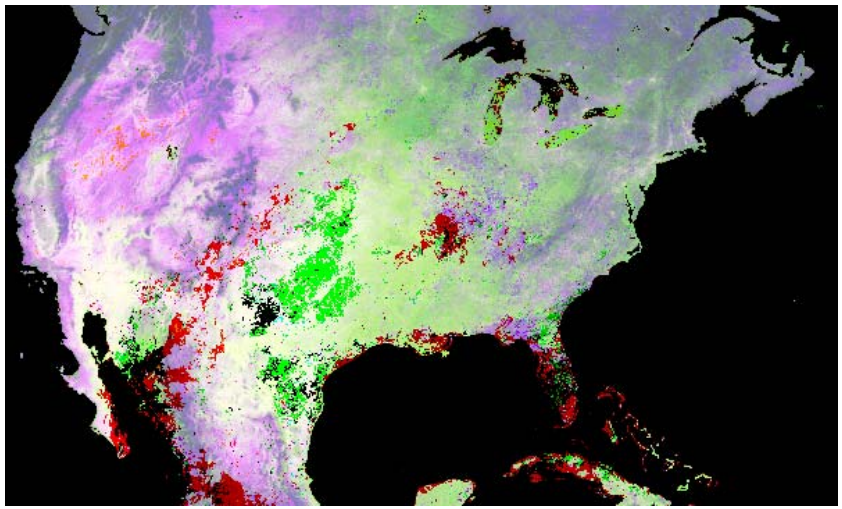

Fig. 3(a)

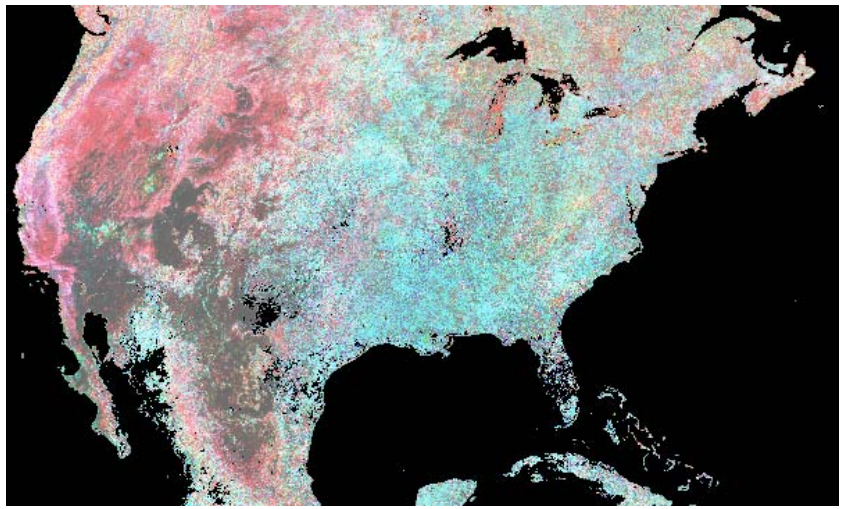

Fig. 3(b)

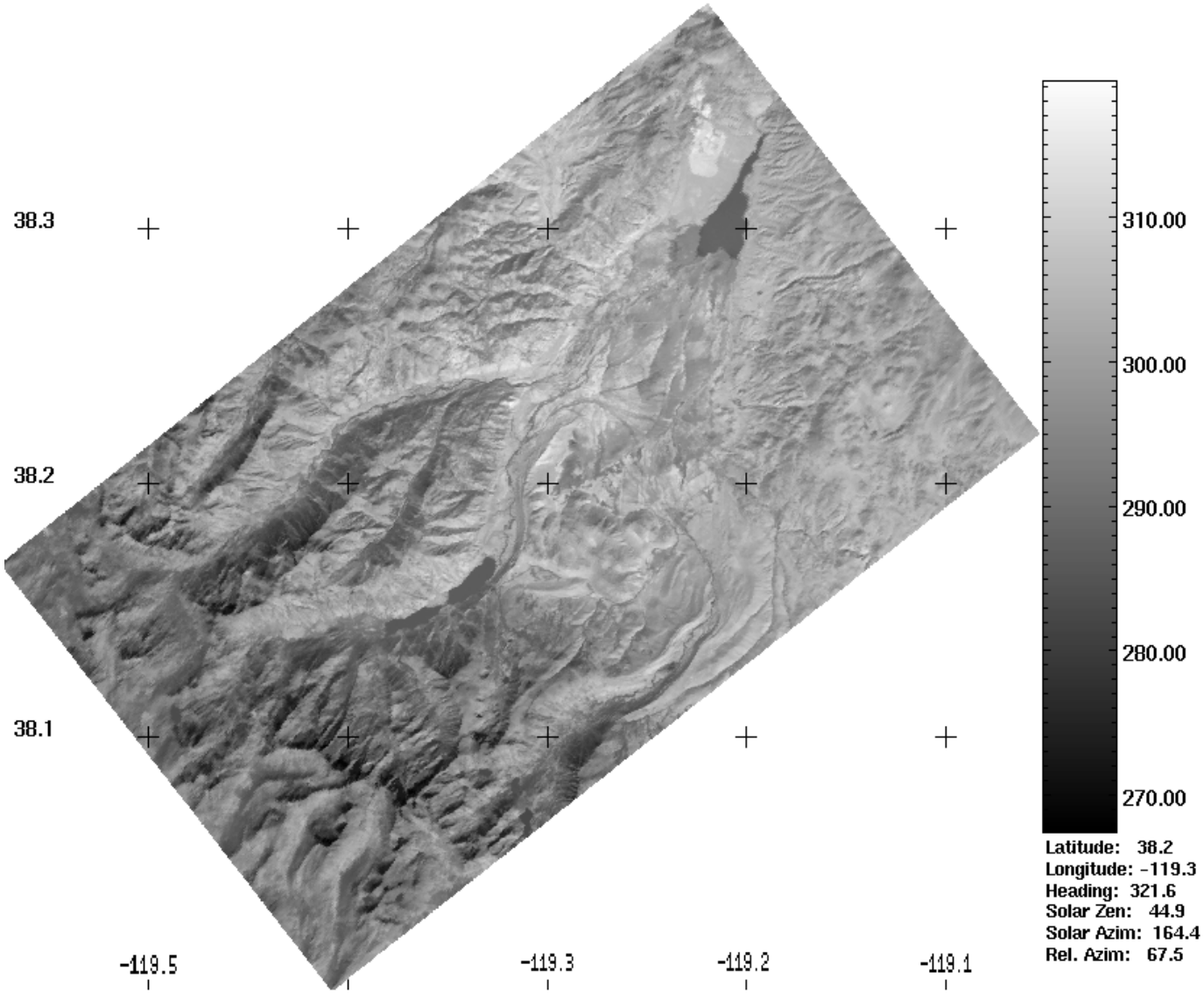
38.3
38.2
38.1
-119.5
-119.3
-119.2
-119.1
310.00
300.00
290.00
280.00
270.00
Latitude: 38.2
Longitude: -119.3
Heading: 321.6
Solar Zen: 44.9
Solar Azim: 164.4
Rel. Azim: 67.5

Fig. 4

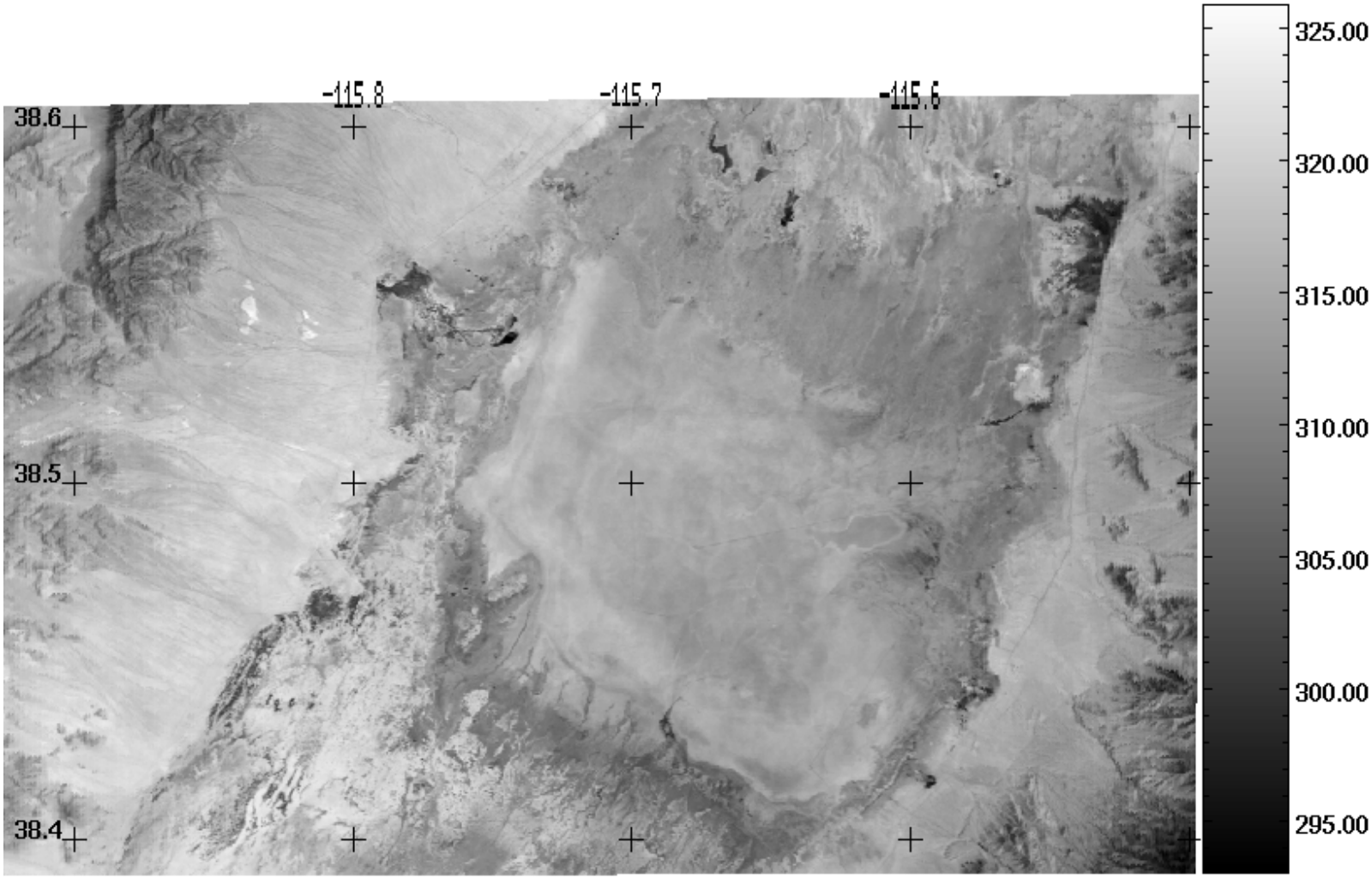
-115.8
-115.7
-115.6
38.6
38.5
38.4
325.00
320.00
315.00
310.00
305.00
300.00
295.00

Fig. 5

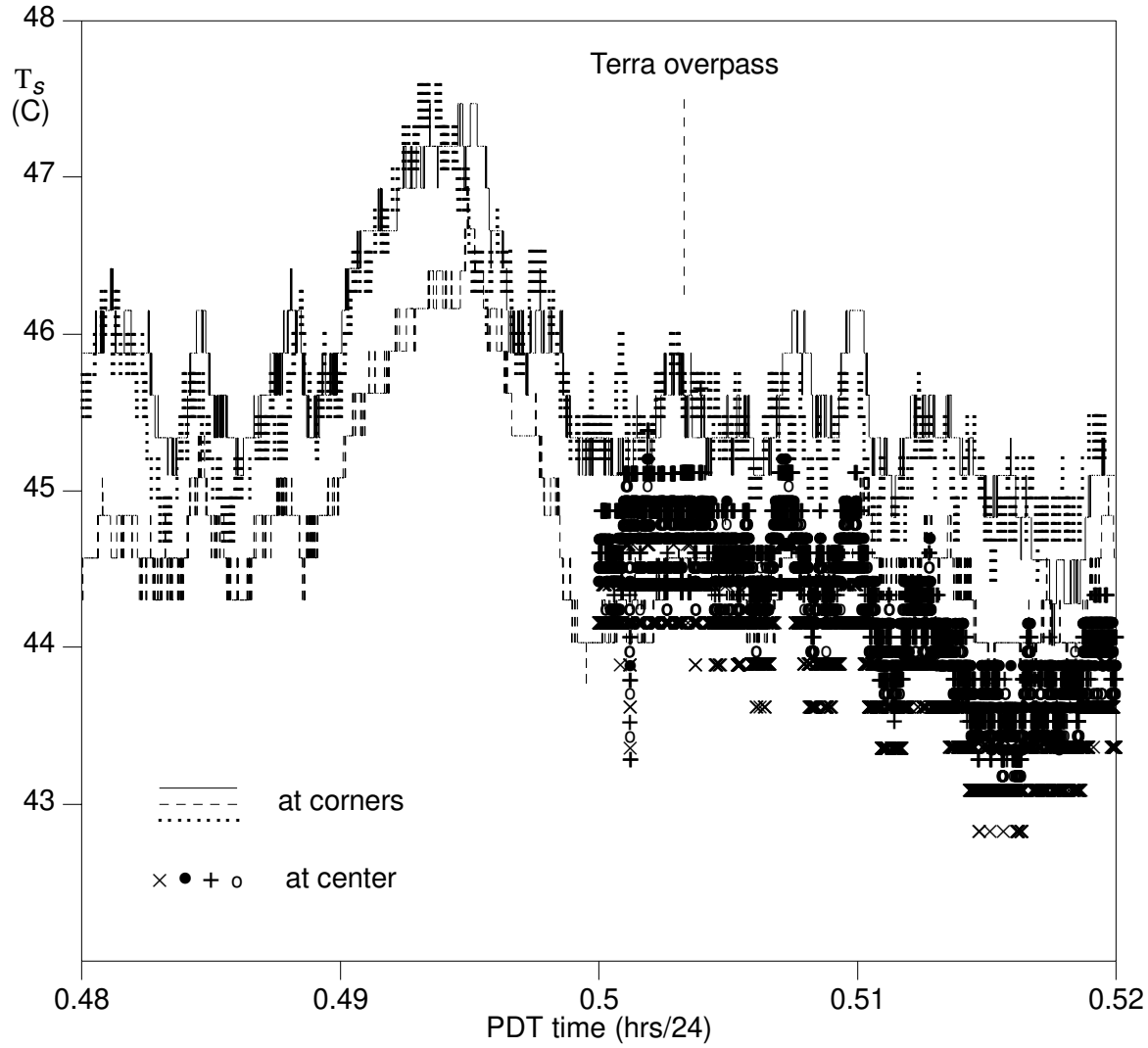

Fig. 6, Surface temperatures measured by 7 radiometers in Railroad Valley, NV on 21 July 2001.

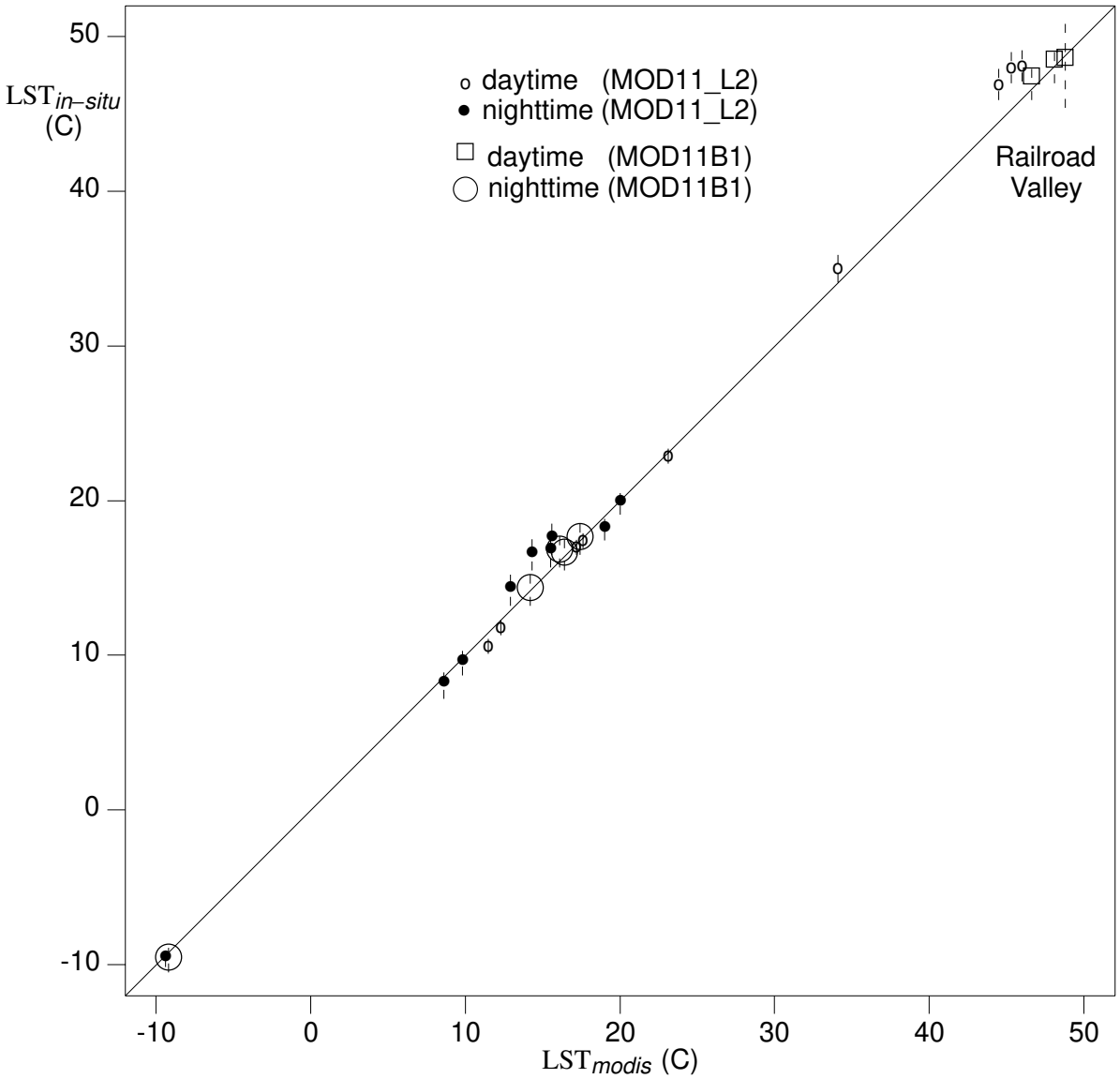

Fig. 7, Comparison between the MODIS LSTs and the LSTs from in-situ measurements.